



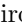




# Coherent coupling of momentum states: selectivity and phase control

Charlie Leprince <sup>\*</sup>, Victor Gondret , Clothilde Lamirault , Rui Dias ,  
Quentin Marolleau <sup>†</sup>, Denis Boiron , and Christoph I. Westbrook   
*Université Paris-Saclay, Institut d'Optique Graduate School,  
CNRS, Laboratoire Charles Fabry, 91127, Palaiseau, France*

We demonstrate the effect of pulse shaping in momentum selective atomic Bragg diffraction. We compare temporal square pulses, which produce sidelobes in momentum space, with other shapes which can produce more nearly square momentum distributions. We produce pulses that simultaneously address two sets of velocity classes and demonstrate that we can control the differential phase imprinted on them in a way that is insensitive to laser phase fluctuations. Our work marks a significant step forward in testing Bell inequalities using massive particles entangled in momentum.

## I. INTRODUCTION

The coherent coupling of quantum states is central to many quantum technologies including quantum computation, simulation and sensing [1]. Depending on the specific application, this coupling must typically be optimized according to various criteria such as efficiency, selectivity, speed or immunity from noise. Here we will discuss a common example, the coupling of different atomic momentum states using Bragg diffraction or momentum selective Raman transitions [2, 3].

These coupling mechanisms can be understood as two-photon transitions producing transfers between two well defined momentum classes. In the Raman case, the momentum transfer is accompanied by a transition between two low lying states in a three-level system. They are basic techniques in atom interferometry as well as being a spectroscopy technique for many body physics [4]. Laser beams producing the transfer are typically pulsed on for some duration and roughly speaking, the duration determines the momentum selectivity of the pulse. Bragg diffraction has been used to perform atomic Hong-Ou-Mandel and other interferometry experiments which are working towards a Bell inequality test with momentum entangled atoms [5–8]. In these experiments, both the momentum selection and the control of the wavepacket phase are crucial. A pulse whose temporal profile is square results in a momentum response containing sidelobes and which is not flat near the center of the efficiency curve. These drawbacks can be mitigated by choosing more complex pulse shapes. Some authors have investigated the use of Gaussian pulse shapes [9–11] and polychromatic frequency spectra [12] while others have used optimal control techniques [13–17] to improve various aspects of interferometer performance. While highly effective couplings can be engineered through optimal control techniques, the cost function used for the optimization is very specific and the resulting waveform is complex. Pulse shaping protocols were pioneered in the context of NMR [18, 19] and have recently found some

applications in atom interferometry [20–22]. These earlier methods have the advantages of being general, with analytical forms and depending on a small number of parameters. However, they require changing the sign of the two-photon Rabi frequency during the pulse, which is technically challenging.

In this article we report the experimental realization of these pulse shaping techniques in the context of atomic Bragg diffraction. We first demonstrate our ability to efficiently address atoms in a given momentum class while suppressing the coupling to others. We also extend these ideas to implement a simple and effective method to simultaneously address two sets of momentum classes and control their relative phase.

## II. MODEL AND CALCULATIONS

Bragg diffraction can be understood as a two-photon transition coupling momenta separated by  $2\hbar k$ , with  $k = \frac{2\pi}{\lambda} \sin \frac{\alpha}{2}$ , where  $\alpha$  is the angle between the beams, each characterized by a frequency  $\omega_i$ , a phase  $\varphi_i$ , and a Rabi frequency  $\Omega_i$ . In the rotating frame, two momenta are coupled by an interaction Hamiltonian:

$$\frac{\Omega_R(t)}{2} e^{i\delta t} |p\rangle \langle p + 2\hbar k| + h.c. \quad (1)$$

where  $h.c.$  denotes the Hermitian conjugate, and  $\Omega_R$  is the two-photon Rabi frequency, defined as

$$\Omega_R = \frac{\Omega_1 \Omega_2^*}{2\Delta} = \frac{|\Omega_1| \cdot |\Omega_2|}{2\Delta} e^{i\varphi_L} \quad (2)$$

with  $\varphi_L = \varphi_1 - \varphi_2$  the laser phase difference. We also define the two-photon detuning  $\delta$

$$\hbar\delta = \hbar(\omega_2 - \omega_1) - \left( \frac{2\hbar^2 k^2}{m} + \frac{2\hbar k}{m} p \right) \quad (3)$$

which is assumed to be small compared to  $\Delta$ , the one-photon detuning from the excited state. The doublet is resonantly coupled when the frequency difference  $\omega_2 - \omega_1$  and the momentum  $p$  are such that  $\delta = 0$ . Off resonant doublets are still coupled, but their transfer efficiencies

<sup>\*</sup> Contact author: [charlie.leprince@protonmail.com](mailto:charlie.leprince@protonmail.com)

<sup>†</sup> Present address Qblox, Delftechpark, Netherlands.

are lower, a point which is of central importance for this article.

Given an atom in an initial momentum state  $|p\rangle$ , the above interaction Hamiltonian takes the atom to the state  $c_p |p\rangle + c_{p+2\hbar k} |p + 2\hbar k\rangle$ . Assuming that  $\delta$  is constant and that  $c_{p+2\hbar k}$  remains small, 1st order perturbation theory predicts

$$c_{p+2\hbar k}(\delta) \propto \int_0^t dt' \Omega_R(t') e^{i\delta t'} \quad (4)$$

meaning that the deflection coefficient  $c_{p+2\hbar k}$  as a function of the detuning is proportional to the Fourier transform of the pulse  $\Omega_R$  as a function of time. Thus a square pulse results in a momentum space profile in the form of a sinc function ( $\text{sinc}(x) = \sin x/x$ ). Conversely, one can realize a transfer with a nearly square profile in momentum space by having the atoms interact with a laser pulse whose profile is a sinc function.

When the fraction of transferred atoms  $|c_{p+2\hbar k}|^2$  is large, Eq. 4 is not exact; however we will show that even for a 50% or 100% transfer, a sinc is a simple and effective pulse shape in our conditions. In the following, we will denote  $\Omega_M$  as the magnitude of the two-photon Rabi frequency, so that a square pulse corresponds to  $\Omega_R(t) = \Omega_M$  during the pulse and  $\Omega_R(t) = 0$  otherwise. According to the Fourier relationship (see Eq. 3 and 4), the selected momentum spectrum contains sidelobes at momenta inversely proportional to the duration of the pulse. A temporal sinc pulse in the interval  $[0, T]$  is given by:

$$\Omega_R(t) = \Omega_M \text{sinc}(\Omega_S(t - T/2)). \quad (5)$$

In order to produce a deflector (100% transfer) one chooses  $\Omega_S = \Omega_M$  so that the time integral of the Rabi frequency is  $\pi$ . For a 50-50 beam splitter one chooses  $\Omega_S = 2\Omega_M$ . The use of a sinc pulse has the advantage, compared to optimal control methods, of being intuitive and having a simple analytical form. One can also realize more complex pulse shapes, see Eq. 6 and Fig. 3.

In the above discussion, it is assumed that there is no diffraction into higher orders, *i.e.*, that we remain within the so-called *Bragg* regime [3]. This limits the peak power of the beams, so that the peak transfer energy  $\hbar\Omega_M$  remains below the two photon recoil energy  $\hbar^2 k^2/m$ . This condition, where only two diffraction orders are coupled, can be readily checked experimentally by counting atoms at momentum  $p - 2\hbar k$ ,  $p + 4\hbar k$ , and so on. Numerically, calculations are conducted using a multi-level model where levels are coupled two by two through the interaction Hamiltonian from Eq. 1, *i.e.* without making a two-level approximation.

### III. EXPERIMENTAL SETUP

In our experiment, we use a metastable helium Bose-Einstein Condensate (BEC) in two geometries, shown in

Fig. 1. The vBEC is in an optical dipole trap and is elongated along the  $z$  direction hence has a narrow velocity distribution along this axis [23] – indeed its width is negligible for what follows. We make use of this BEC to perform the spectroscopy measurements. The hBEC is in a magnetic trap elongated along  $x$  and has a broad velocity distribution along the vertical axis  $z$  [24]. A 1083 nm laser, red-detuned by  $\Delta/2\pi = -800$  MHz from the  $2^3S_1 \rightarrow 2^3P_0$  transition is split into two beams that intersect at the atomic cloud with a vertical angle of  $\alpha = 31^\circ$ . The Bragg velocity is therefore  $2\hbar k/m = 49.6$  mm/s along the vertical axis. With this detuning and the pulse durations used, excitation to the electronically excited state is negligible. To generate the modulated Bragg pulses, the power is controlled by an acousto-optic modulator (AOM) common to both beams and locked to a reference signal using a feed-back loop with a 70 kHz bandwidth (Fig. 1). The relationship between the (two-photon) Rabi frequency and the power is calibrated using Rabi oscillations.

To produce a sinc-shaped two-photon Rabi frequency, the laser power at the output of AOM 0 is controlled to be proportional to  $|\Omega_R(t)|$  with  $\Omega_R(t)$  of Eq. 5, and a  $\pi$  phase shift is added whenever the Rabi frequency changes sign (see Fig. 1).

## IV. EXPERIMENTAL RESULTS

### A. Pulse shaping results

After producing the vBEC, we turn off the trap and allow the cloud to expand for 1 ms. We then apply a velocity independent Raman pulse to transfer the atoms from the  $m_J = 1$  state to the  $m_J = 0$  state, rendering the falling cloud insensitive to magnetic field gradients, while the 1 ms expansion reduces the effect of interactions. We then apply the Bragg pulse, including a frequency chirp to compensate the acceleration due to gravity. After diffraction, the atoms fall 46 cm onto a Micro-Channel Plate (MCP) detector [25] which records the arrival times and transverse positions of individual atoms. The  $\sim 300$  ms time of flight is long enough that the detected times and positions correspond to the 3 dimensional velocities of the atoms after the diffraction pulse. Due to the narrow velocity distribution (3 mm/s), the cloud is uniformly diffracted into momentum states with an upward Bragg velocity and barely expands along the vertical axis during the time of flight. The diffracted atoms fall onto the MCP about 5 ms after the undiffracted atoms.

To illustrate the effect of pulse shaping, we scan the frequency difference  $\omega_2 - \omega_1$ , hence the detuning  $\delta$ , and observe the fraction of diffracted atoms for several pulse shapes. The results are shown in Figs. 2 and 3 and compared to theoretical expectations, computed without any fit parameter by integrating the Schrödinger equation using the coupling Hamiltonian defined in Eq. 1 for a multi-

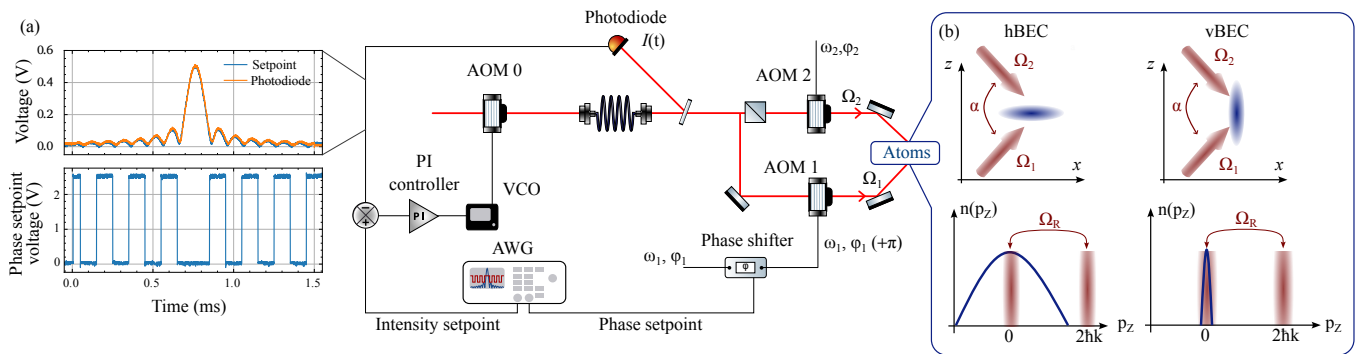


Figure 1. (a) Schematic diagram of the modulation technique to produce a sinc-shaped excitation. PI denotes Proportional Integral, VCO is Voltage-Controlled Oscillator and AWG Arbitrary Waveform Generator. The two plots show the waveforms used to produce a sinc excitation. The phase shifter used is a Mini-Circuits SPHSA-251+ component. Upper panel: intensity waveform produced by AOM 0. Lower panel: phase shift applied to AOM 1. 2.5 V corresponds to a  $\pi$  phase shift. (b) The hBEC is highly confined along the vertical direction hence has a broad momentum distribution, much larger than the typical width of the Bragg pulses used here. Thus only a part of the distribution is transferred. The vBEC has a narrow distribution along  $z$  and thus acts as a spectroscopic probe of the laser pulse distribution.

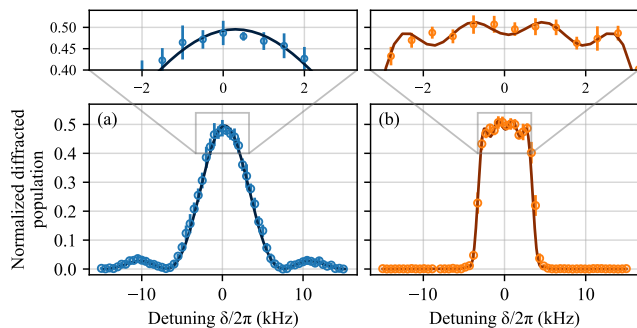


Figure 2. Experimental (dots) and theoretical (solid lines) transfer efficiency of a beam splitter for a square pulse (a) and a sinc pulse (b) where 1 kHz in detuning corresponds to 2 mm/s in velocity. The theoretical expectations are computed from the Schrödinger equation using the Hamiltonian given in Eq. 1 without any fit parameter, and integrated over a range of 1 kHz to account for the experimental binning range. Parameters are  $\Omega_M/2\pi = 1.88$  kHz and durations of 133  $\mu$ s and 1 ms respectively for the square and sinc pulses.

level model.

For a 50% transfer, which can be thought of as a beam splitter, we compared a square pulse in panel (a) of Fig. 2 with a sinc pulse in panel (b) with the same two-photon Rabi frequency (and therefore the same peak power). Although the fraction of transferred atoms is not small, we observe that the sinc pulse eliminates the side-lobes and leads to an almost square profile. The rising and falling slopes of the sinc pulse are 4 times greater than for the square pulse. The resonance width, which we define to be the range over which the transferred fraction is close to 1/2 (between 47.5 and 52.5%), is greater for the sinc pulse by a factor of 1.5. The results are in very good agreement with the expected theoretical profiles in terms of width,

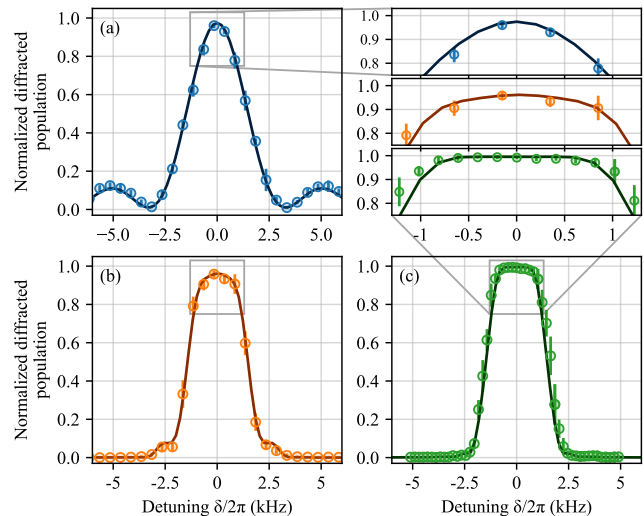


Figure 3. Experimental (dots) and theoretical (solid lines) transfer efficiency of a deflector for a square pulse (a), a sinc pulse (b) and a reburp pulse (c). The theoretical expectations are integrated over a range of 1 kHz to account for the experimental binning range. Parameters are  $\Omega_M/2\pi = 1.88$  kHz and a duration of 266  $\mu$ s for the square pulse,  $\Omega_M/2\pi = 2.05$  kHz and a duration of 1.5 ms for the sinc pulse, and  $\Omega_M/2\pi = 0.57$  kHz and a duration of 1.8 ms for the reburp pulse. For the reburp pulse, all points in the interval  $[-0.5$  kHz, 0.5 kHz] are better than 98%.

efficiency, and spectral shape. Although it was not used to obtain the data in Fig. 1, pulse shaping also lends itself easily to apodization which would help to further flatten the spectrum for the sinc pulse.

We perform the same experiment for a pulse with 100% transfer (a momentum deflector). We compared a square pulse to a sinc pulse and to a so called *reburp*

pulse [26] which was identified in the context of NMR [18, 19] and theoretically studied for Bragg diffraction in Ref. [21]. The reburp pulse is defined in terms of a Fourier series as

$$\Omega_R(t) = \Omega_M \left[ A_0 + \sum_{n=1} A_n \cos(n\Omega_S t) \right] \quad (6)$$

for  $0 \leq t \leq 2\pi/\Omega_S$ , where  $\Omega_S = 2A_0\Omega_M$  and the  $A_n$  are coefficients up to the 15th order [27]. Like the sinc, this pulse also undergoes sign changes.

The parameters of the three pulses (power and duration) were chosen so as to have the same half width in momentum. The results are plotted in Fig. 3. It is observed that for the sinc pulse, the deviations from the Fourier relationship shown in Eq. 4 become significant. Although not giving a square spectrum, the sinc still reduces the sidelobes and gives a sharper and flatter profile than the square pulse: the slopes at a 50% transfer are 1.8 times greater for the sinc pulse, while the resonance width (defined here as the range for which there is at least a 95% transfer) increases by a factor of 1.5 compared to the square pulse. The reburp pulse leads to a momentum deflector for which the resonant momentum range is wider (by a factor of 2 compared to the square pulse), flatter, and sharper (the rising and falling slopes are 2 times greater than the square pulse) than the others. We know of no equally effective pulse shapes in the case of 50% transfer.

### B. Application: dual coupling

Pulse shaping also allows one to select two distinct momentum doublets from a distribution. This can be achieved with a single pair of Bragg beams modulated by a cosine function. In the case of a sinc pulse, we have:

$$\Omega_R(t) = \Omega_M \text{sinc}[\Omega_S(t - T/2)] \cos[\Omega_D t/2] \quad (7)$$

From the interaction Hamiltonian given in Eq. 1, one can see that a two-photon Rabi-frequency  $\Omega_M e^{i\Omega_D t/2}$  results in an effective detuning which will shift the resonance by  $\Omega_D/2$ . Therefore multiplying any given pulse by a cosine induces a resonance with two momentum doublets, provided that the duration of the pulse is long enough. The frequency  $\Omega_D$  controls the separation between the selected momentum doublets.

We illustrate in Fig. 4 this process experimentally using the hBEC for two values of  $\Omega_D$ . As expected, there are two resonant velocity classes, separated by  $\Delta v = \Omega_D/(2k)$ . Using the vBEC, we tested this technique over a large range of  $\Omega_D$  and confirmed the expected linear variation of the selected velocity class difference by varying the detuning between the two Bragg beams. The frequency difference between the observed resonance peaks as a function of  $\Omega_D$  is fitted, and we find a linear relationship with a slope of 1.02(4),

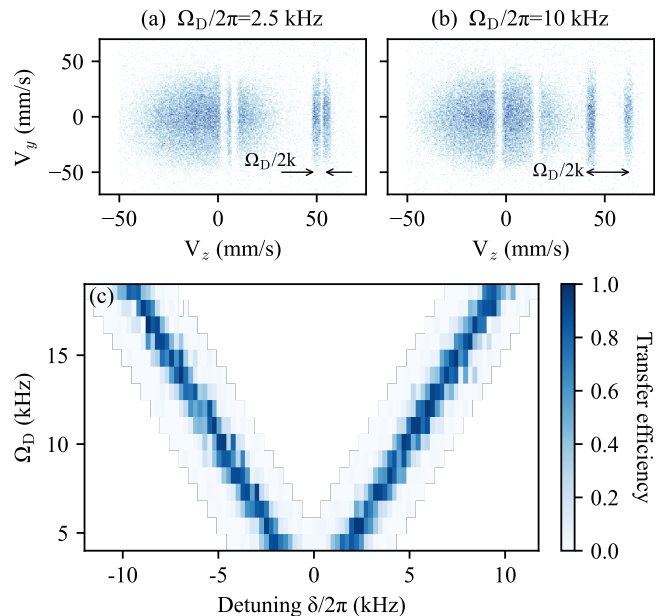


Figure 4. Effect of an overall modulation of the diffraction pulse. Two velocity doublets are selected by the same pulse ( $\Omega_M/2\pi = 1.5$  kHz,  $T = 1.5$  ms) and the separation is controlled by the modulation frequency  $\Omega_D$ . (a-b) A modulation frequency of  $\Omega_D/2\pi = 2.5$  kHz leads to a velocity difference of 5 mm/s in (a) while a modulation frequency of  $\Omega_D/2\pi = 10$  kHz leads to a velocity difference of 20 mm/s in (b). Data is averaged over 50 experimental runs with hBEC. (c) The transfer efficiency of vBEC (color scale) is shown as a function of the detuning. Each slice shows a different modulation frequency.

which confirms that the modulation frequency  $\Omega_D$  indeed controls the resonance difference.

### C. Differential phase control

We can also tune the phase imprinted on the atomic wave packets. To this end, a phase parameter  $\theta$  can be added to the modulation function:

$$\Omega_R(t) = \Omega_M \text{sinc}[\Omega_S(t - T/2)] \cos[(\Omega_D t + \theta)/2] \quad (8)$$

where  $\theta$  controls the relative phase imprinted between the two selected momentum doublets through its contribution to the phase in Eq. 2. The phase imprinted is  $\varphi_L \pm \theta/2$ , depending on the considered momentum doublet.

To investigate this phase imprinting effect, we have realized an interferometer using the Bragg pulses. In the following, the procedure will be described in two main steps. First, we will describe the interferometer and the results that were obtained using unmodulated pulses as defined in Eq. 5. The observation of an interference patterns aims at confirming that a stable phase can be im-

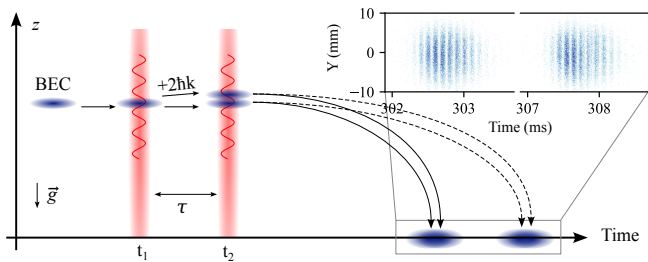


Figure 5. Diagram of the interferometer used to test the phase stability of the Bragg pulses. Two  $\pi/2$  pulses create four falling clouds interfering two by two when they overlap at the detector. The fringe period depends on the value of the interferometer time  $\tau$ . The inset displays fringes observed with the interferometer for  $\tau = 2$  ms. The color encodes the density as a function of the arrival time  $T$  defined in Eq. 9 and the horizontal position  $Y$ . Data is averaged over 25 repetitions: the good contrast confirms the stability of the phase difference for a duration of the order of  $\tau$ .

printed on the atoms. Second, we will show that the use of modulated pulses like in Eq. 8 thereby realizes two parallel interferometers, each involving a different momentum doublet. The objective here is to ensure precise control over the phase difference between these two doublets through the pulse shape parameter  $\theta$ .

*Un-modulated pulses:* The interferometer consists of two consecutive beam splitter pulses, as shown in Fig. 5. An hBEC is first split into two parts by a beam splitter sinc pulse similar to that in Fig. 2. After a time  $\tau$ , a second identical pulse is applied and the resulting four clouds fall on the detector. Two clouds with the same momentum after the second pulse ( $p$  or  $p + 2\hbar k$ ) have a spatial separation of  $2\hbar k\tau/m$  much smaller than their spatial width, so they overlap. Since they did not acquire the same phase during their fall, the two clouds interfere and produce fringes while falling on the detector. The interference pattern depends on a phase  $\Phi$  given by

$$\Phi = 2kg\tau T + \phi_1 - \phi_2 + \phi_{\text{grav}} \quad (9)$$

where  $g$  is the acceleration of gravity,  $T$  the arrival time at the detector,  $\phi_i$  the phase imprinted by each pulse on the atoms ( $i = 1$  or  $2$ ) and  $\phi_{\text{grav}}$  is a constant related to the phase difference accumulated during the fall, which depends on  $\tau$  but not  $T$ .

In Fig. 5 we show the interference patterns corresponding to two overlapping clouds for a wait time of  $\tau = 2$  ms, obtained using two successive sinc beam splitters with  $\Omega_M/2\pi = 5$  kHz. The fringes show high contrast even when averaged over 25 repetitions. For each Bragg pulse, the phase  $\phi_i$  imprinted by the pulse is the phase difference  $\varphi_L$  between the lasers, so the stability of the fringes confirms that the laser phase difference is stable on a timescale of 2 ms.

The fringes can be shifted at will by adding a voltage to the phase shifter during the second pulse. We observe

that the atomic phase  $\Phi$  varies linearly with the electronically added phase with slope 1.

*Modulated pulses:* More importantly, when using pulses modulated by a cosine function as in Eq. 8, we create two parallel interferometers  $A$  and  $B$  involving different momentum doublets, see Fig. 6. For the first pulse, we use  $\theta = 0$ , leading to  $\phi_1^A = \phi_1^B = \varphi_L$ . For the second pulse, we add a phase at the origin  $\theta/2$  to the cosine modulation function. We denote  $A$  (resp.  $B$ ) the momentum doublet resonant whose resonance was shifted by  $+\Omega_D/2$  (resp.  $-\Omega_D/2$ ). Phases  $\pm\theta/2$  are therefore imprinted on the two momentum doublets with opposite signs. The phases  $\phi_2$  in Eq. 9 are given by:

$$\phi_2^A = \varphi_L + \theta/2 \quad \text{and} \quad \phi_2^B = \varphi_L - \theta/2 \quad (10)$$

where the laser phase difference  $\varphi_L$  was shown to remain constant over the time scale of the interferometer. Therefore we have:

$$\phi_1^A - \phi_2^A = \theta/2 \quad \text{and} \quad \phi_1^B - \phi_2^B = -\theta/2 \quad (11)$$

such that the fringes from each resonant doublet are shifted in opposite directions when varying  $\theta$ , in a way that is independent of the two laser phases.

Panel (a) of Figure 6 shows the resulting fringes. As expected, we observe four regions exhibiting interference fringes, corresponding to two parallel interferometers. The interference patterns in region  $A$  centered at an arrival time of 296 ms and region  $B$  centered at 298 ms are respectively shifted by  $\pm\Omega_D/2$  relative to the resonance that would be obtained without modulating the Rabi frequency. In order to verify that a different phase is indeed imprinted on these two momentum doublets, we fit the interference patterns for different values of  $\theta$ . The phase of the interference pattern is plotted as a function of  $\theta$  in panels (d) and (e) of Fig. 6 for each of these clouds. The slopes of the linear fits as a function of  $\theta$  are  $+0.50(2)$  for  $A$  and  $-0.51(2)$  for  $B$ . This confirms that the phase at the origin  $\theta$  of the pulse shaping modulation function controls the relative phase imprinted between the two selected velocity classes.

The ability to control the relative phase of two parallel beam splitters is of particular importance in an experiment such as that of Ref. [6]. In that experiment, it was necessary to control the relative phase of two simultaneously applied beam splitters. This was done with a single beam splitter and a broad range of velocities. The relative phase shift was related to the detuning of each velocity class and was not under the experimentalists control. With a dual beam splitter as demonstrated in Fig. 6, this phase is under control. In addition, we have performed simulations of a Bell inequality experiment and shown that not only is the phase controlled but also that the phase remains nearly constant over the velocities inside a given momentum doublet ensuring that all the atoms in the doublet contribute to the Bell signal [28].

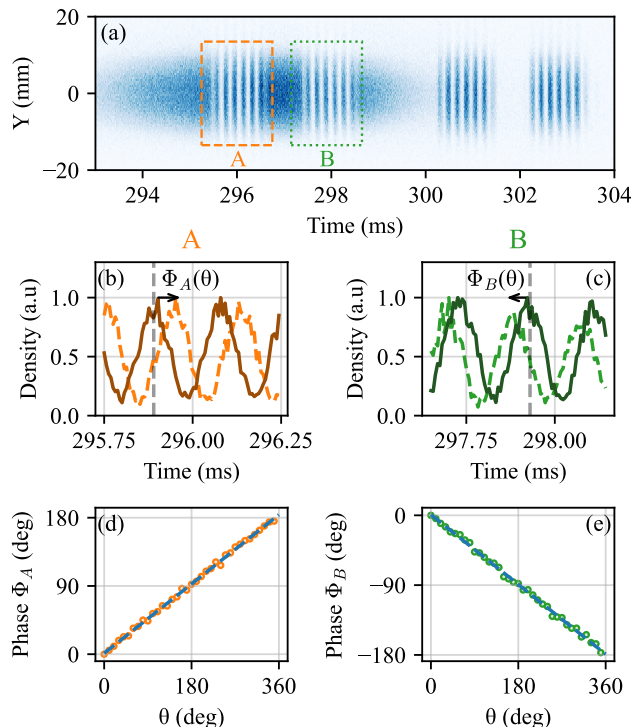


Figure 6. (a) Interference fringes from two parallel interferometers, which are produced by modulated  $\pi/2$  pulses as in Eq. 7. Data averaged over 350 experimental runs, conducted with a modulated sinc pulse with  $\Omega_M/2\pi = 5$  kHz,  $\Omega_D/2\pi = 10$  kHz,  $\tau = 4$  ms. (b-c) We zoom on the interference region A in (b) and B in (c) to show the fringes for a phase  $\theta = 0$  (solid line) and  $\theta = \pi/2$  (dashed line). The phase of the interference patterns shifts with  $\theta$ . (d-e) Phase of the interference pattern as a function of  $\theta$ , for the interference region A (d) and for the interference region B (e). A linear fit yields slopes of  $+0.50(2)$  for A and  $-0.51(2)$  for B. The parameters used for these two plots are  $\Omega_M/2\pi = 1.5$  kHz,  $\Omega_D/2\pi = 10$  kHz,  $\tau = 1$  ms.

## V. CONCLUSION

We have demonstrated precise control over the reflectivity of Bragg diffraction using shaped pulses. Our experimental setup provides access to negative or even complex two-photon Rabi frequencies, thereby enhancing the selectivity and reflectivity characteristics of Bragg transfers. For beam splitters, a sinc pulse produces a square-shaped spectrum, while for deflectors, a reburp pulse yields a more nearly square profile than a sinc pulse. These pulses offer the advantage of being parameter-sparse and easily adaptable to various experimental conditions.

By modulating a pulse with a cosine function, dual Bragg coupling with resonances with two momentum doublets can be achieved. An interferometry experiment further demonstrates fine control over the phase difference imprinted between each momentum doublet, ensuring that this difference remains, by design, independent of the phases of the lasers used. This is of particular interest when trying to act differently on two momentum classes that are very close spatially.

## ACKNOWLEDGMENTS

We are grateful to Marc Cheneau and Paul Paquiez for their early contributions to the development of this setup. The research leading to these results has received funding from QuantERA Grant No. ANR-22-QUA2-000801 (MENTA) and ANR Grant No. 20-CE-47-0001-01 (COSQUA), the LabEx PALM (ANR-10-LABX-0039PALM), Région Ile-de-France in the framework of the DIM SIRTEQ program, and Quantum Paris-Saclay.

- 
- [1] C. L. Degen, F. Reinhard, and P. Cappellaro, Quantum sensing, *Rev. Mod. Phys.* **89**, 035002 (2017), arXiv: 1611.02427.
  - [2] A. Miffre, M. Jacquy, M. Büchner, G. Tréneç, and J. Vigué, Atom interferometry, *Phys. Scr.* **74**, C15 (2006).
  - [3] A. D. Cronin, J. Schmiedmayer, and D. E. Pritchard, Optics and interferometry with atoms and molecules, *Rev. Mod. Phys.* **81**, 1051 (2009).
  - [4] R. Ozeri, N. Katz, J. Steinhauer, and N. Davidson, *Colloquium: Bulk Bogoliubov excitations in a Bose-Einstein condensate*, *Rev. Mod. Phys.* **77**, 187 (2005).
  - [5] R. Lopes, A. Imanaliev, A. Aspect, M. Cheneau, D. Boiron, and C. I. Westbrook, Atomic Hong–Ou–Mandel experiment, *Nature* **520**, 66 (2015).
  - [6] P. Dussarrat, M. Perrier, A. Imanaliev, R. Lopes, A. Aspect, M. Cheneau, D. Boiron, and C. I. Westbrook, Two-Particle Four-Mode Interferometer for Atoms, *Physical Review Letters* **119**, 173202 (2017).
  - [7] D. K. Shin, B. M. Henson, S. S. Hodgman, T. Wasak, J. Chwedeńczuk, and A. G. Truscott, Bell correlations between spatially separated pairs of atoms, *Nature Communications* **10**, 4447 (2019).
  - [8] K. F. Thomas, B. M. Henson, Y. Wang, R. J. Lewis-Swan, K. V. Kheruntsyan, S. S. Hodgman, and A. G. Truscott, A matter-wave Rarity–Tapster interferometer to demonstrate non-locality, *Eur. Phys. J. D* **76**, 244 (2022).
  - [9] H. Müller, S.-w. Chiow, and S. Chu, Atom-wave diffraction between the Raman-Nath and the Bragg regime: Effective Rabi frequency, losses, and phase shifts, *Phys. Rev. A* **77**, 023609 (2008).
  - [10] B. Fang, N. Mielec, D. Savoie, M. Altorio, A. Landragin, and R. Geiger, Improving the phase response of an atom interferometer by means of temporal pulse shaping, *New J. Phys.* **20**, 023020 (2018).
  - [11] X. Zhao, X. Liu, J. Sun, Z. Xu, Z. Hu, and X. Yang, Optimized Gaussian pulse for mirrors and beam splitters

- in atom interferometry, *Eur. Phys. J. D* **76**, 39 (2022).
- [12] S. Lellouch, O. Ennis, R. Haditalab, M. Langlois, and M. Holynski, Polychromatic atom optics for atom interferometry, *EPJ Quantum Technol.* **10**, 9 (2023).
- [13] W. G. Alway and J. A. Jones, Arbitrary precision composite pulses for NMR quantum computing, *Journal of Magnetic Resonance* **189**, 114 (2007).
- [14] J. Saywell, M. Carey, N. Dedes, I. Kuprov, and T. Freegarde, Efficient state-symmetric beamsplitters and mirrors for atom interferometers using optimized pulses, *J. Phys. B: At. Mol. Opt. Phys.* **55**, 205501 (2022).
- [15] J. C. Saywell, M. S. Carey, P. S. Light, S. S. Szigeti, A. R. Milne, K. S. Gill, M. L. Goh, V. S. Perunicic, N. M. Wilson, C. D. Macrae, and others, Enhancing the sensitivity of atom-interferometric inertial sensors using robust control, *Nature Communications* **14**, 7626 (2023).
- [16] N. Dedes, J. Saywell, M. Carey, I. Kuprov, and T. Freegarde, Optimizing beam-splitter pulses for atom interferometry: A geometric approach, *Phys. Rev. A* **108**, 053319 (2023).
- [17] G. Louie, Z. Chen, T. Deshpande, and T. Kovachy, Robust atom optics for Bragg atom interferometry, *New J. Phys.* **25**, 083017 (2023).
- [18] H. Geen and R. Freeman, Band-selective radiofrequency pulses, *Journal of Magnetic Resonance* (1969) **93**, 93 (1991).
- [19] S. McDonald and W. S. Warren, Uses of shaped pulses in NMR: A primer, *Concepts Magn. Reson.* **3**, 55 (1991).
- [20] A. Dunning, R. Gregory, J. Bateman, N. Cooper, M. Himsworth, J. A. Jones, and T. Freegarde, Composite pulses for interferometry in a thermal cold atom cloud, *Phys. Rev. A* **90**, 033608 (2014).
- [21] Y. Luo, S. Yan, Q. Hu, A. Jia, C. Wei, and J. Yang, Contrast enhancement via shaped Raman pulses for thermal coldatom cloud interferometry, *Eur. Phys. J. D* **70**, 262 (2016).
- [22] Y. Wang, J. Cheng, Y. Liu, and T. Lin, Amplitude-modulated mirror pulses for improved cold-atom gravimetry, *Phys. Rev. A* **109**, 053501 (2024).
- [23] G. B. Partridge, J.-C. Jaskula, M. Bonneau, D. Boiron, and C. I. Westbrook, Bose-Einstein condensation and spin mixtures of optically trapped metastable helium, *Phys. Rev. A* **81**, 053631 (2010).
- [24] A. Robert, O. Sirjean, A. Browaeys, J. Poupard, S. Nowak, D. Boiron, C. I. Westbrook, and A. Aspect, A Bose-Einstein Condensate of Metastable Atoms, *Science* **292**, 461 (2001).
- [25] M. Schellekens, R. Hoppeler, A. Perrin, J. V. Gomes, D. Boiron, A. Aspect, and C. I. Westbrook, Hanbury Brown Twiss Effect for Ultracold Quantum Gases, *Science* **310**, 648 (2005).
- [26] Re-BURP stands for Refocusing Band-Selective Pulse with Uniform Response and Phase.
- [27] The coefficients used are  $A_n = [0.48, -1.03, 1.09, -1.59, 0.86, -0.44, 0.27, -0.17, 0.10, -0.08, 0.04, -0.04, 0.01, -0.02, 0.00, -0.02]$ . The peak Rabi frequency is 6.24 times  $\Omega_M$ .
- [28] C. Leprince, *Phase control and pulse shaping in Bragg diffraction for quantum atom optics: from matter-wave interferences to a Bell's inequality test*, *Ph.D. thesis*, Université Paris-Saclay (2024).